Journal of
Ceramic Science
and Technology

J. Ceram. Sci. Tech., **05** [02] 101-114 (2014)
DOI: 10.4416/JCST2013-00029
available online at: http://www.ceramic-science.com

Experimental Characterization and Thermomechanical Modelling of Microstructure Interactions in Cellular Carbon Magnesia Refractories

G. Falk*[1], A. Jung[1], W. da Silveira[1], S. Diebels[2]

[1]Universität des Saarlandes, Research Group Structural and Functional Ceramics, Campus C6 3, D-66123 Saarbrücken, Germany
[2]Universität des Saarlandes, Institute of Applied Mechanics, Campus C6 3, D-66123 Saarbrücken, Germany
received October 18, 2013; received in revised form December 27, 2013; accepted March 31, 2014

Abstract

Experimental results and computational solutions regarding microstructural interactions and their influence on the thermomechanical strength of cellular carbon foams reinforced with yttria-stabilized zirconia (YSZ) and silicon carbide (SiC) coatings are presented. The computational approach is related to the quantification of failure stresses as a function of the microstructural size under thermal shock loading and under hot bending with microstructural-based finite element analysis. The numerical results of this simplified computational approach are correlated to the experimentally motivated Hasselman's equations. Correlated to the computational results, these experimental result parameters for final crack length and final crack density allow conclusions to be drawn about the most suitable microstructural foam parameters in order to achieve advanced thermal shock characteristics for next-generation hybrid carbon foam refractories.

Keywords: Porous carbon, thermal shock, FEM modelling

I. Introduction

The vision of research in next-generation carbon-containing refractories is the development and optimization of innovative high-temperature materials and their combinations as multifunctional advanced ceramic components with extraordinary characteristics in terms of microstructural design, material processing, and material sustainability [1,2,3]. More specifically, increased demands in steelmaking processes require carbon refractories with improved functionalities, and improved compatibility and interaction between slag and high-quality steel in high-temperature applications [4]. Thus, investigating carbon-containing refractories with increased service life, improved thermal shock resistivity, and increased corrosion and oxidation resistivity represents one of the key development goals of modern carbonized refractory materials [5].

Most recently, methods and approaches for achieving these objectives imply the use of carbon foams [6]. Today carbon foams and cellular carbon matrices are produced from alternative precursors; coal-tar- or petroleum-based pitches as well as synthetic resins such as Novolacs and Resoles [7,8,9,10,11,12]. Carbon foams are today ranked among the well-established engineering and functional ceramic materials for various high-temperature applications owing to their superior thermal conductivities as well as high absorption rates of thermal radiation [13,14,15,16,17,18]. In the framework of recent studies, hybrid carbon-foam magnesia composites open up the potential for advanced thermal shock characteristics, provided specific microstructural criteria are met [19,20]. Since the definition of thermal shock resistivity can be different for specific assumptions and material parameters, the following conclusions could serve as a basic understanding of thermal shock behaviour of brittle materials.

Refractory materials are subjected to quasistatic and also sudden high thermal loading, e.g. when a furnace is heated up or molten metal is poured into a cold ladle in the steel making industry. These conditions cause large, thermally induced stresses that could lead to early failure of the refractories. There are two kinds of thermally induced stresses: permanent and temporary thermal stresses. Permanent thermal stresses only occur in heterogeneous materials, where the constituents differ in their coefficient of thermal expansion (CTE). Wherever no gradients in temperature are present, e.g. in quasistatic heating of a furnace, the only possible thermal stresses are permanent thermal stresses owing to the coupling of materials with a mismatch in their CTEs. Temporary thermal stresses arise in homogeneous and also heterogeneous materials when temperature gradients are formed. Temporary stresses disappear at temperature balance if the material is only linear-elastically deformed by the thermal stress. If there is a sudden change in temperature owing to spontaneous thermal surface loading with the formation of large temperature gradients, this is called thermal shock. Damage accompanied by permanent thermal stresses is called thermal damage and originates from the isotropic thermal expansion of constituents that differ in the CTE. Damage occurring

* Corresponding author: g.falk@nanotech.uni-saarland.de

from temporary thermal stresses is based on temperature gradients leading to spatially constrained elastic expansion and arises not only in heterogeneous but also in homogeneous materials. This elastic-driven damage is called mechanical damage. Total damage is a combination of both thermal and elastic damage [21,22].

The initiation of thermal shock cracking is therefore commonly described by the merit index of $\sigma_f/E\alpha$ [23-27]. Alternatively, Hasselman's approach defines thermal shock resistivity as the ratio of the fracture energy for crack initiation to the fracture energy for continuous crack propagation [28]. Despite other approaches concerning the definition of different thermal shock parameters under specific boundary conditions, it is meanwhile common knowledge that suitable microstructural and geometrical parameters have to be coupled with local thermal fields in order to be able to proceed with reliable prediction and verification of thermal shock resistivity [29,30,31]. Nevertheless, the development and design of advanced thermal-shock-resistant hybrid carbon foam refractories is still challenging considering that experimental as well as theoretical and numerical studies should contribute to thermal shock prediction as a function of geometrical and microstructural parameters as well as local thermal boundary conditions.

It follows that thermal, e.g. CTE [32,33] or thermal conductivity, and mechanical parameters, e.g., Young's modulus or failure stresses [34], of carbon foam matrices have to be adapted and designed as a function of quenching temperature ΔT in order to achieve advanced thermal shock characteristics. At the same time, a coherent and comprehensive approach, aimed at making the computational prediction of thermal shock behaviour of hybrid carbon foams available, involves taking into account the following general understanding.

Cellular materials like foams are so-called microheterogeneous materials, which consist of two or even three different hierarchical construction levels. According to this hierarchical structure in both experiments and computational modelling, their behaviour could be described on different scales, where the construction elements of the lower scales are not resolved and the regarded scale is treated as a homogeneous continuum. The description of complete samples or compounds takes place on the macro scale, that of single pores or a small number of pores on the meso scale, and the resolution of single struts on the micro scale. Based on this, most foam properties depend on both intrinsic (meso scale: e.g. pore size) and extrinsic measures (macro scale: sample size). Hence, size effects, arising from a reduction in the microstructural construction elements, play a significant role in the mechanical behaviour of microheterogeneous materials like foams [35,36,37,38].

Two different approaches are mainly pursued in modelling microheterogeneous materials: phenomenological and micromechanical models. Phenomenological models describe macroscopic properties with purely mathematical model parameters, the exact identification of which requires extensive experimental investigations. Micromechanical models illustrate the properties under consideration of the microstructure and physical mechanisms with structural mechanical calculations [39,40,41,42,43]. Micromechanical models in the description of the macroscopic behaviour offer the advantage of the explicit consideration of the microstructure by microstructural constitutive equations. This is, however, combined with the disadvantage of a tremendous increase in computation time. In contrast, the use of phenomenological models guarantees the computational modelling of large-scale problems with low effort [44,45,46,47].

Cellular refractory materials, e.g. periclase (MgO)-filled carbon foams [6,19,20,48] are also microheterogeneous materials. Modelling refractories leads to thermomechanical-coupled problems. Starting from the description of thermal shock parameters defined by Hasselman [28,49,50,51] and the thermal shock fracture criterion from Lu and Fleck [52], there have been different approaches to modelling thermal shock and transient thermomechanical damage in refractory materials. Whereas with analytical models[53,54,55,56] to calculate the effect of thermal shock it was only possible to describe very simple-shaped refractories, using the finite element method [57,58,59,60,61], the evolution of thermally induced stresses by modelling refractory components and parts of them was possible. Hence, with the help of finite element analysis the design of such components could be improved in order to reduce the stresses and effect a prolonged lifetime.

Despite the brittle behaviour of refractories, first-stage computational models were based on linear elastic fracture mechanics. A second step was the incorporation of phenomenological crack models for quasi-brittle materials and their extension with higher gradients in order to model size effects [62,63].

Advanced continuum mechanical models for the thermomechanical characterization of refractories are based on damage mechanics. Prompt *et al.* [64] describe thermoelastic damage with one single variable for both compressive and tensile damage. More recent models [65,66,67,68,69,70] suggest a multiplicative split for the two types of thermally induced stresses and damage. Damhof *et al.* developed a non-local thermal shock damage model with an additive combination of elasticity-based damage from isotropic expansion by a mismatch in the CTE of different constituents and, in the case of thermal damage arising from localized constrained expansion owing to temperature gradients, according to the assumption that both damage mechanisms act independently on different scales [21,22,57]. The elastic damage works macroscopically causing elastic strains due to temperature gradients leading to internally and externally constrained thermal expansion. The thermal damage caused by isotropic thermal expansion due to homogeneous temperature changes causes damage as a result of the mismatch in the CTE between the different constituents. Thus, thermal damage works on the micro scale [21,22].

It was the primary objective of this study to gain an understanding of how thermal stresses applied to carbon

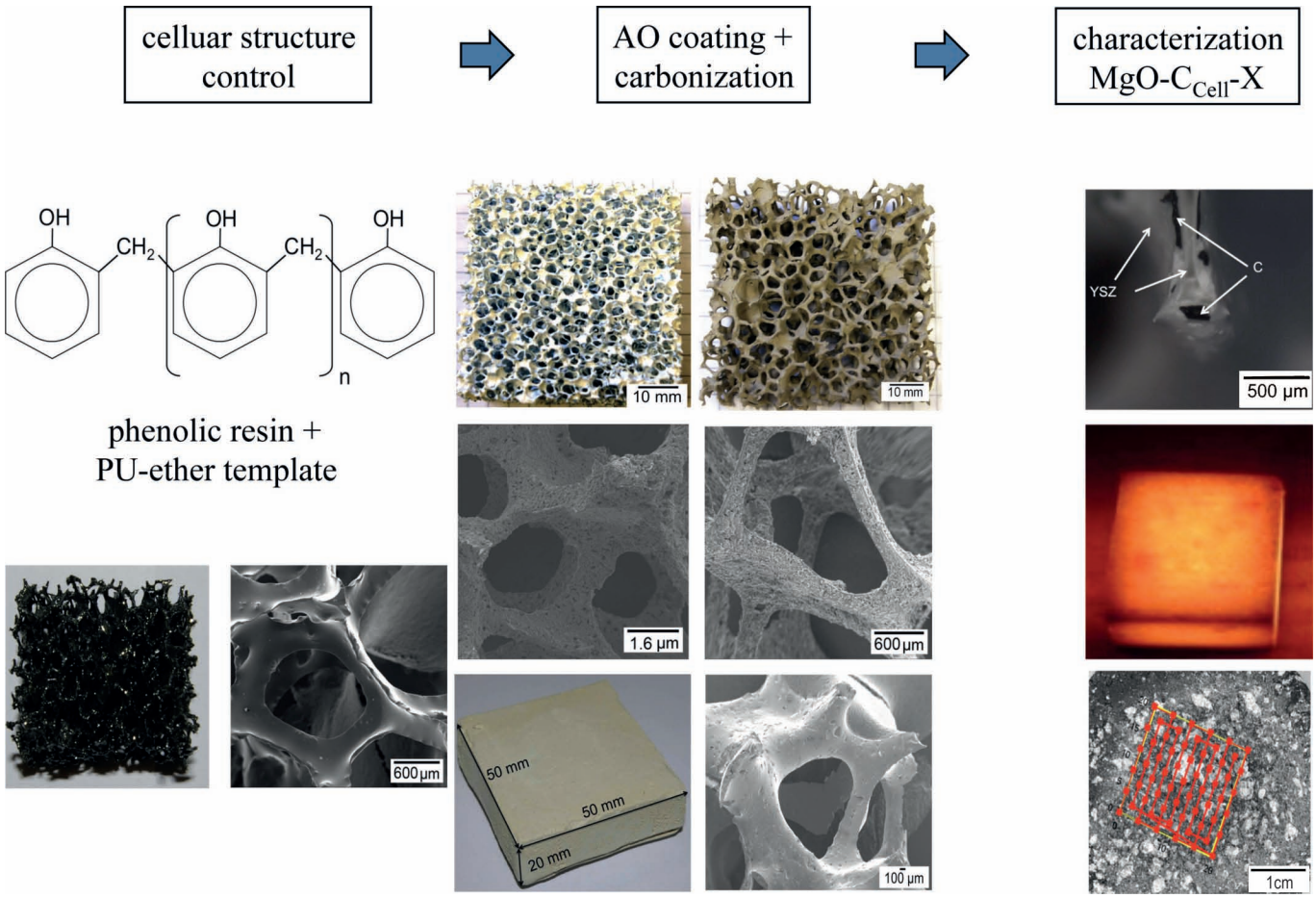

Fig. 1 : Scheme of carbon hybrid foam processing steps incorporating a high-temperature periclase phase.

foam hybrid materials create critical crack conditions and disintegration and to identify design parameters, more specifically cell size, density as well as carbon strut coatings made of yttria-stabilized zirconia (YSZ) and silicon carbide (SiC) that would allow advanced thermal shock resistivity. Therefore, experimental parameters such as Young's modulus and cold crushing strength (CCS) have been implemented into an extended Hasselman's approach to thermal shock derivation. The result parameters final crack length and final crack densities allow conclusions to be drawn about the most suitable microstructural foam parameters.

In addition to the experimental verification of quenching thermal shock parameters and the hot bending tests, microstructural-based finite element analysis has been performed to study the effect of changes in the microstructural size of cellular MgO-C refractories in order to reduce permanent and temporary thermally induced stresses to prolong the lifetime of components made of refractory materials.

The computational approach is related to the quantification of failure stresses as a function of the size of the microstructure, and for the hot bending tests, also as a function of the temperature. Similar to the early stages of thermomechanical modelling of refractories, the MgO-C hybrid foam is modelled by linear elasticity. The maximal occurring tensile stresses are used as failure criteria.

II. Experimental Description

(1) Materials and carbon hybrid foam preparation

The scheme of cellular carbon matrix MgO-C refractory processing is illustrated in the following figure (see Fig. 1). The subsequent processing steps are as follows:

Slurries were made from a mixture of 50 wt% ethanol and 50 wt% Novolak resin powder (Bakelite PF 0227 SP 01, Hexion); the slurry was dispersed in a dissolver (Dispermat N1/SIP, VMA Getzmann GmbH, Germany) without additional additives; the polymeric foam replication process was performed by immersion of 10 ppi (*pores per inch*) PU sponges (ISP GmbH, Limburg, Germany) in the Novolak-Ethanol slurry; the excess slurry was removed using controlled compression in order to improve the distribution of the remaining slurry; and samples were left to dry at room temperature for 12 h. Heat treatment of the samples in an electric tubular furnace in argon was performed in one stage process; a temperature of 500 °C was maintained for 4 h at a heating rate of 2 K/min for the pyrolysis of the PU polymer, superimposed by the transformation of the resin to a glassy carbon phase. The as-synthesized samples are designated as "reticulated vitreous carbon" (RVC).

The subsequent coating of carbon foams was performed by gel-casting processing. The gel-casting solution was prepared with 1.5 wt% κ-carrageen (Koenig & Wiegand, Germany) as gelling additive, 1.5 wt% corn flour (Werz, Germany) as thickening agent, 0.8 wt% Antiprex A40 (Ciba Inc., Basel, Switzerland) as dispersing agent. The

67 wt% YSZ and SiC solutions were prepared by mixing YSZ and SiC and additives with demineralized water followed by heating at a temperature of 80 °C under atmospheric pressure for 10 min. RVC infiltration of the cellular template foam substrates was performed with the prepared dispersions. The excess solution was subsequently removed.

The processing of hybrid carbon foams incorporated with a high-temperature periclase phase was performed by the infiltration of periclase slurries in the open porous carbon foam network at room temperature. Slurries were made from a mixture of 50 wt% double distilled water and 50 wt% MgO (Type TA-3, Lehmann & Voss & Co., Hamburg, Germany). The slurry was dispersed in a dissolver without other additives. The slurries were cast into the open porous RVC-YSZ/SiC reticulated structures and dried at room temperature for 24 h. The cast samples were respectively coked at 1 000 °C in a graphite granules bed.

Specific characteristics of the five different carbon hybrid foam specifications are provided in Table 1.

Table 1: Parameters of hybrid carbon foams under investigation and pitch-bonded 12C-MgO reference sample (MACARBON L710 F, Refratechnik Steel GmbH, Düssseldorf). The indicated porosity, density, and mean flaw size values correspond to a condition after coking at 1000 °C in argon atmospheres. Porosity and density values of 12C-MgO reference according to [72].

specification	porosity (%)	density (g/cm^3)	mean flaw size (mm)	cell size (ppi)
6C – MgO	36.2	2.19	0.35	non-cellular
$6C_{cell}$ – MgO	38.5	2.11	2.5	10
$6C_{cell}$ – Y SZ – MgO	37.9	2.15	4.2	10
$6C_{cell}$ – SiC – MgO	42.9	1.96	4.3	10
12C – MgO	10.39	3.03	0.25	non-cellular

(2) Modelling of crack initiation and crack propagation energy for refractories

Moduli of elasticity (E_{PGM}) were approximated using the Pabst-Gregorova model [30, 71], which takes a specific porosity-MoE correlation into account. For further simplification, it is assumed that the starting point of the release of elastic energy, e.g. by crack formation, is strongly influenced by the specific Young's modulus and the porosity of the as-processed materials. Based on these theoretical assumptions, the flexural strength and the tensile strength are correlated for this specific linear elastic problem according to the following expression:

$$\sigma_{f,th.} = \frac{P \cdot S}{B \cdot W^2} = \sigma_{f,th.} \cdot C^* = \varepsilon_{th} \cdot E_{PGM} \cdot C^* \quad (1)$$

with $\varepsilon_{th} = \text{const.}$

The parameters W, B, S and P correspond to the width, thickness, span width of the bearings of the three-point bending set-up and the external load, respectively. In this specific case the correlation parameter C^* of the flexural and tensile strength was set to "1".

The geometry correction factor is defined according to ASTM E-399 by the following equation:

$$f\left(\frac{l_0}{W}\right) = 3 \cdot \sqrt{\frac{l_0}{W}} \cdot \frac{1.99 - \left(\frac{l_0}{W}\right) \cdot \left(1 - \frac{l_0}{W}\right) \cdot \left[2.15 - 3.93\frac{l_0}{W} + 2.7\left(\frac{l_0}{W}\right)^2\right]}{2\left(1 + 2\frac{l_0}{W}\right)\left(1 - 2\frac{l_0}{W}\right)^{2/3}} \quad (2)$$

For the estimation of a theoretical critical stress intensity factor $K_{IC,\,th.}$, under the assumption of a straight crack line of the length l_0 in a sample of the width, W = 25 mm, the thickness, B = 25 mm, and the span width, S =125 mm, the following expression is applied:

$$K_{IC,th.} = \frac{P \cdot S}{B \cdot W^2} \cdot \sqrt{W} \cdot f\left(\frac{I_0}{W}\right) \quad (3)$$

The moduli of elasticity and the estimated critical stress intensity factors were the basis for calculating the theoretical energy for crack initiation $\gamma_{NBT,th.}$ with the following expression:

$$\gamma_{NBT,th.} = \frac{K^2_{IC,th.}}{2 \cdot E_{PGM}} \quad (4)$$

The theoretical average energy needed for unit crack propagation during period from crack initiation, $\gamma_{WOF,th.}$ – that also depends on the load-displacement curve, the projected fracture area perpendicular to the tensile stress direction and the width W, the thickness B and the initial crack length l_0 of the material – can be specified with the help of these parameters for the first approximation:

$$\gamma_{WOF,th.} = \frac{\int_0^{\delta^*} P d\delta}{A_{fracture}} \approx \frac{0.5 P_{max}\, \delta}{B(W - I_0)} \quad (5)$$

The underlying variable δ^* denotes the maximum displacement of the sample under a load in a three-point bending setup documented by the load-displacement curve.

(3) Thermomechanical characterization and thermal shock parameter assessment

In order to model the impact of the mean porosity, mean density and the modulus of rupture on thermal shock resistivity and micro-/macro crack as well as defect density after a singular thermal shock treatment at a specific temperature gradient ΔT_C by heating up the samples from room temperature up to 1 000 °C, a mathematical concept is applied. This mathematical approach is extensively described in [29].

It is postulated that the flexural strength after thermal shock corresponds to the MOR values measured at room temperature after thermal shock tests at a critical temperature difference ΔT_C. Based on this assumption, the final crack length l_f was calculated with the Griffith equation. The modelling and theoretical calculation of the final crack length after the thermal shock tests are based on the following expression:

$$K_{IC,th.} = MOR \cdot \sqrt{I_f \pi} \cdot f\left(\frac{I_0}{W}\right) \quad (6)$$

$$I_f = \frac{1}{\pi}\left[\frac{K_{IC,th.}}{MOR \cdot f\left(\frac{I_0}{W}\right)}\right]^2 \quad (7)$$

After a singular thermal shock test the MOR values correspond to the mean flaw size values l_0 given in Table 1. The modulus of rupture of the refractory specimen was determined according to DIN EN 993 – 6 by measuring the amount of force applied to a rectangular test piece of specific dimensions 150 x 25 x 25 mm (L x W x B) until failure occurs.

The Young's modulus after thermal shock is estimated according to the following equation:

$$E_{thermal} = \frac{\sigma_C (1 - \nu)}{\alpha \Delta T} = \frac{MOR (1 - \nu)}{\alpha \Delta T} \quad (8)$$

A mean linear coefficient of thermal expansion (CTE, α) of $15.1 \cdot 10^{-6}$ K^{-1} is assumed within the applicable temperature range from 293 K to 1273 K. Poisson ratio ν is set as 0.2 in each thermal shock boundary condition case.

Significant contributions to the calculation of the final volumetric density of cracks after singular thermal shock treatment are provided by the Poisson ratio ν, the initial crack length l_0, the final crack length after thermal shock treatment l_f, as well as the fracture surface energy ratio $\gamma_{NBT}/\gamma_{WOF}$. In order to estimate the microstructural impact on thermal shock resistivity and micro/macro crack as well as defect density after a singular thermal shock treatment at a specific temperature gradient ΔT_C, the mathematical model elaborated in [29] enables the estimation of the final volumetric density of cracks N_f according to the following equation:

$$N_f = \left[\left(\frac{\gamma_{NBT}}{\gamma_{WOF}}\right)\frac{3 (1 - 2\nu)}{8 (1 - \nu^2)}\frac{1}{I_f^2 I_0}\right] \quad (9)$$

Additionally, the cold crushing strength (CCS) was measured at room temperature according to DIN EN 993 – 5 after a singular thermal shock test within the temperature range between room temperature and 1 000 °C. The test specimen with a diameter of ∅36 mm and a height of 36 mm was prepared by means of dry cutting.

The critical temperature difference values ΔT_C to initiate crack propagation for short cracks were calculated according to [29] with the following equation:

$$\Delta T_C = \left[\frac{\pi \gamma_{NBT} (1 - 2\nu)^2}{2 E \alpha^2 (1 - \nu^2) I_0}\right]^{1/2} \quad (10)$$

The hot modulus of rupture (HMOR) values were determined according to DIN 51048/1 (EN 993 – 7) at 1 000 °C in argon atmospheres. The experiments were carried out with three-point HMOR testing apparatus. The dimensions of all the specimens for the HMOR characterization were 150 x 25 x 25 mm (L x W x H). Finally, the applied loading rate for HMOR testing in the machine was 0.02 MPa/s and 0.15 MPa/s respectively. The final temperature of HMOR was 1 000 °C at a heating rate of 5 K/min with a soaking time of 30 min.

For the calculation of the fracture surface energy for crack propagation, γ_{WOF}, it is assumed that the $\gamma_{NBT}/\gamma_{WOF}$ ratio amounts to a fixed value of 0.2. It has to be mentioned that the values for this ratio can go down to 0.1 in the case of exceptionally high-thermal-shock-resistant refractory materials.

The theoretical background and computational methodologies of Finite Element based thermomechanical modelling are subsequently illustrated and discussed in detail in the following paragraph.

III. Theory and Modelling

(1) 2D microstructural modelling approaches

We made the assumption that the behaviour of vitreous carbon and periclase remains linear elastic in the investigated temperature regime. In order to study the influence of changes in the microstructural size on the thermal shock behaviour and on the failure behaviour under bending of quasistatic-heated MgO-C hybrid foams, a microstructural 2D linear elastic model of a cellular two-phase MgO-C refractory is investigated by transient and static-coupled temperature-displacement finite element analysis in Abaqus™. The microstructure of a MgO-filled vitreous carbon foam is built up in 2D with hexagonal unit cells representing the glassy carbon phase and a central circular MgO phase made of the periclase modification. The reference unit cell consists of a regular hexagon with an edge length d_{strut} of 3.5 mm and an inner circle with a diameter d_{pore} of 5 mm for the second phase. These structural parameters correspond to a 10 ppi foam. Whereas the periclase pore phase contains only to one unit cell, the struts of the carbon foam structure are only built by the merging of two unit cells at each edge (see Fig. 2a). To study the effect of changes in the microstructural size, the reference unit cell, defined as 100 % type, is shrunk to 50 % and 25 % respectively. The RVEs of the three different microstructural sizes are represented in Fig. 2b.

Two types of computational experiments were performed: first, the influence of changes in the microstructural size on the thermal shock behaviour of MgO-C hybrid foams was studied; and second, the failure behaviour of quasistatic-heated MgO-C hybrid foam samples under bending load was investigated. The RVE structures as well as the bending samples are stress-free at ambient temperature. The models are meshed by triangular first order plain-strain shell elements (CPE3T) with a global element size of 0.5 mm, 0.15 mm, and 0.12 mm for the reference unit cell, the 50 % type, and the 25 % type, respectively. The used material parameters of vitreous carbon and MgO periclase (see Table 2) are taken partially from literature and partially from the experimental section. For the simplicity of the model, it is assumed that the CTEs of the constituents are temperature independent – the CTE of carbon and periclase differ by one order of magnitude. Hence, for the thermal shock experiments, failure in the investigated cellular MgO-C hybrid refractories occurs by thermal and by elastic mechanical damage. In the bending experiments, failure occurs only by thermal damage due to permanent thermal stresses and by bending stresses.

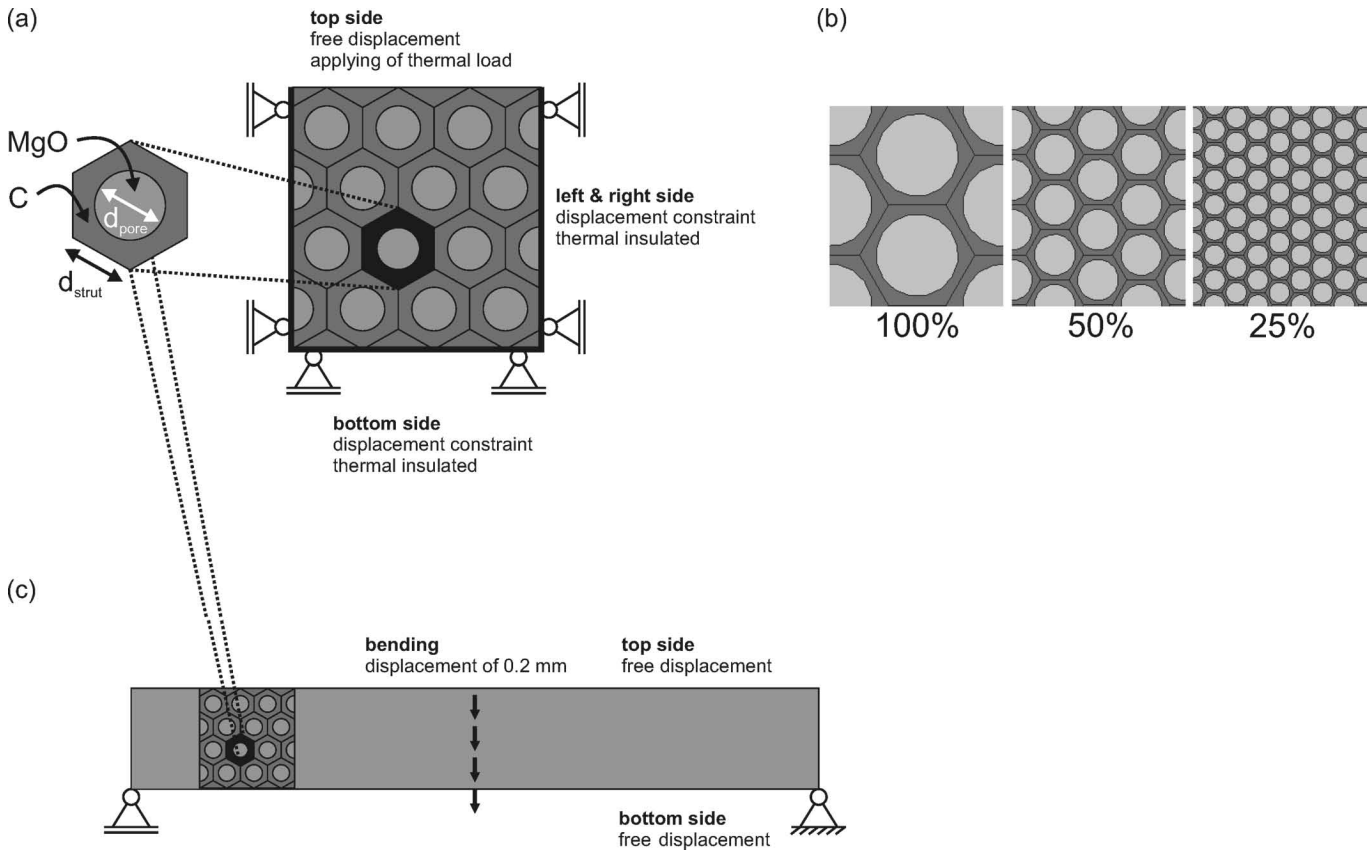

Fig. 2 : Schematic drawing of the reference unit cell and the microstructure of the thermal shock experiments with thermal and mechanical boundary conditions (a), scheme of the three different microstructural sizes (b) and bending samples with mechanical boundary conditions (c).

Table 2: Material parameters of reticulated vitreous carbon (RVC) and periclase used for modelling.

Parameter	RVC	MgO
Density (kg m^{-3})	1450	3580
Young's modulus (GPa)	35	270
Linear CTE ($10^{-6}K^{-1}$)	2.5	1.2
Thermal conductivity (W K^{-1} m^{-1})	5	30
Specific thermal capacity (10^2 J K^{-1} g^{-1})	7.09	10.01
Compressive strength (GPa)	580	2.6
Tensile strength (MPa)	260	220

A rectangular reference representative volume element (RVE) of 48.50 x 52.5 mm (H x W) was built for the investigation of the thermal shock behaviour for each microstructural size. In order to simulate a segment of a larger part of a refractory material thermally loaded on the top side and to prevent rigid body motion, a Dirichlet boundary condition is applied on the left, right, and bottom sides of the RVE by a constrained displacement of the boundary nodes in the normal direction of the three sides and is thermally insulated, whereas the displacement of the top boundary nodes is free and thermal loading is applied on the top boundary nodes (see Fig. 2a). The FE model with transient coupled temperature-displacement analysis was used to simulate the process in the steel making industry, where cold ladles with refractory linings were first heated up from ambient temperature to a temperature of 1 300 °C (1 573 K) to reduce the thermally induced stresses and failure before pouring molten steel at about 1 800 °C (2 073 K) into the ladle in the second step. In order to simulate this whole procedure, two consecutive thermal loading steps were defined. The first step is the quasistatic heating of the RVE from the top side from ambient temperature to 1 573 K for 10.8 h (2 K/min). This step is followed by the thermal shock, where the top side is suddenly thermally loaded with 2 073 K to simulate the pouring of molten steel on the refractory lining. The top boundary reaches the temperature of 2 073 K within 10 s. The thermal shock corresponds to a temperature difference ΔT of 500 K.

To simulate the three-point bending tests of the experimental section, bending samples of 147 x 24 mm (W x H) were constructed from unit cells of the 100 % and 50 %-type, respectively. The lower left and right nodes of the bending beam show a constrained displacement in the y direction, whereas all the rest of the nodes are in free motion. The FE model with static coupled temperature-displacement analysis was used to simulate the bending experiments. The simulation consisted of two consecutive loading steps. The first step is the quasistatic heating of the stress-free bending beam from ambient temperature to 250 °C, 500 °C, 750 °C and 1 000 °C respectively. The second step is the displacement-controlled bending of the heated samples. Here a displacement of 0.2 mm was applied to the nodes on the vertical centre line of the beam. This displacement corresponds to 0.13 % of the beam length.

(2) Computational experiments

The maximal principal stress after the thermal shock loading is computed and linked with the microstructure for the investigation of the thermal shock behaviour. As a criterion of failure, the maximal occurring stresses were chosen and compared with the fracture stresses of vitreous carbon and periclase. According to Table 2, tensile stresses are significantly more critical than compressive stresses. The influence of size effects on the occurring maximal principal stresses has been determined in order to optimize the structural morphology of cellular MgO-C hybrid foams to reduce thermally induced damage. The numerical experiments were evaluated with the maximal principal stresses and according to the Hasselman relation. The classical Hasselman relation uses the residual strength after a thermal shock as a function of the applied temperature reference. Thus the above-mentioned model is linear elastic, there is no loss in fracture strength, and no residual strength could be computed. For the evaluation of the numerical experiments, a Hasselman-like evaluation by plotting the maximal occurring principal stresses as a function of the temperature difference is used.

In the bending experiments, the maximal principal stresses have been determined after the quasistatic heating and bending in order to separate the effects of the thermally induced stresses and bending stresses. Based on the thermal shock experiments, the maximal principal stresses in comparison to the fracture stresses of vitreous carbon and periclase have been used as failure criterion. The determined stresses have been averaged separately for the pores and the struts in the marked regions of Fig. 3.

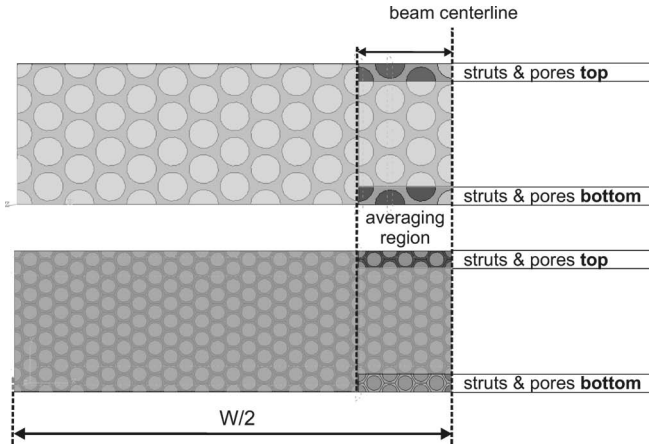

Fig. 3 : Schematic drawing of the left half part of the bending beam with marked regions of stress averaging.

IV. Results and Discussion

(1) Verification of thermomechanical data and thermal shock behaviour

It can be ascertained that the obvious correlation and widely congruent curve progression of the parameters $\sigma_{f,\,th.}$ and $K_{IC,\,th.}$ is caused by the significant influence of the approximated E_{PGM} modulus derived from the Pabst-Gregorova model and thereby by the porosity of the as-processed refractory samples (see Fig. 4a, b). When comparing the MOR and HMOR values a significant reduction of the flexural strength after coking at 1 000 °C is apparent. The maximum temperature of 1 000 °C is justified by the coking reaction and the formation of the glassy carbon phase that prevents the deep penetration of slag in the steelmaking process. (see Fig. 4c).

According to the thermomechanical data, it becomes evident that the approximated $\gamma_{NBT}/\gamma_{WOF}$ ratios significantly influence thermomechanical and thermal shock characteristics of the carbon hybrid foams under investigation (see Fig. 4d). A minimization of the fracture surface energy ratio down to 0.5 is directly connected with significantly reduced volumetric final crack densities after a single thermal shock treatment. Within this specific extended Hasselman's approach, fracture surface energies for crack propagation can exceed values of 100 J/m^2. It follows, according to the experimental and calculated data, that the increased surface fracture energies for crack propagation are correlated with improved thermal shock characteristics.

Analyzing the curve progression of the l_f and N_f values calculated from the thermomechanical data of hybrid carbon foam materials, it is obvious that pitch-bonded noncellular 12C-MgO refractories show a typical R-curve behaviour since the final crack length value is slightly increased in the ΔT_C regime, compared to slightly decreased l_f values within the low-temperature regimes respectively (see Fig. 5).

On the other hand, it is obvious that increased l_f values correspond to elevated K_{IC} data according to the Griffith criteria. As previously discussed, these increased K_{IC} values are directly correlated with increased fracture surface energies γ_{NBT}. With the help of this specifically calculated data, it is assumed that a significant influence of the coefficients of thermal expansion is not considered for the different carbon foam hybrid composites and, due to specific spatial phase distributions and phase anisotropies, gradients of thermal expansion are ignored. This assumption presupposes the requirement that the carbon phase is finely dispersed and has a favourable, i.e. minimizing, effect on the generation of smaller quantities of additional stress gradients. Thereby increased K_{IC} data within the crack propagation stage during the thermal shock treatment sequence is generated. When comparing the thermomechanical characteristics of the hybrid carbon foam materials with those of conventional pitch-bonded 12C-MgO composites, it is characteristic that, besides the decreased $\gamma_{NBT,\,th.}$, $\gamma_{WOF,\,th.}$, and K_{IC} values, a decrease of MOR data is correlated to the overall reduced thermal shock resistivity of the cellular hybride carbon refractories. In this context, the cellular carbon distribution would have minor preference over the statistical distribution of globular pitch-bonded carbon structures. These reduced thermal shock characteristics are mainly caused by the glassy carbon phase instead of the preferred graphite phase, the reduced flexural strength data and the overall reduced modulus elasticity caused by increased porosity. It must, however, be mentioned that the calculated and presumed key parameters particularly aim to evaluate, with practical

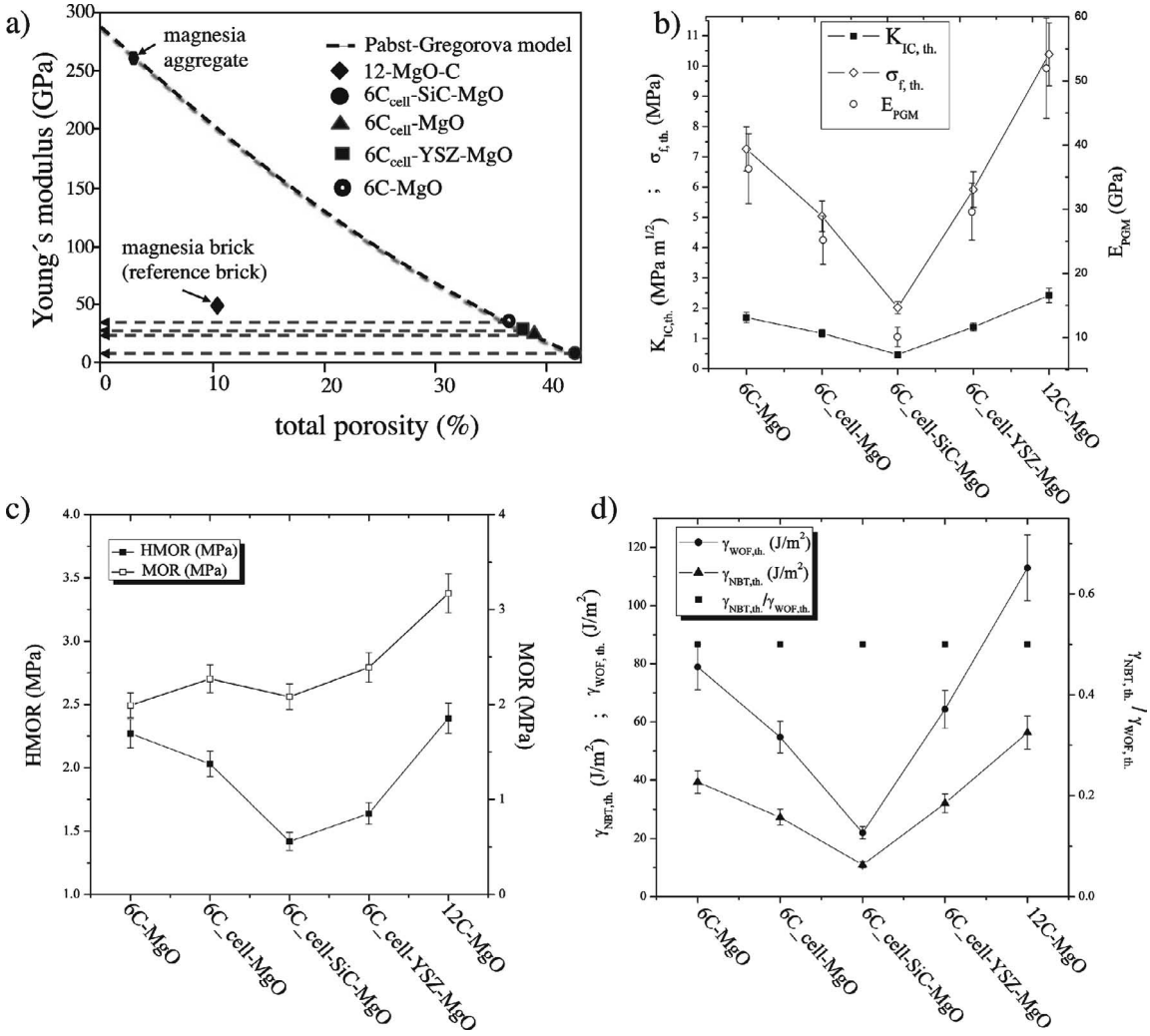

Fig. 4 : Thermomechanical properties of hybrid cellular glassy carbon foams coated with SiC and YSZ layers and infiltrated with MgO matrices as well as a pitch-bonded MgO-C refractory reference material (12C-MgO): Resulting E_{PGM} Young's modulus according to Pabst-Gregorova model (a), theoretical flexural strength $\sigma_{f,th.}$ and theoretical stress intensity factor $K_{IC,th.}$ according to the Eqn. (1) – (4) ($\varepsilon_{th}\cdot C^* = 0.2$, $l_0 = 2$ mm, $f(\frac{l_0}{W}) = 1.47$, $\delta^* = 2.5\cdot10^{-5}$ m) (b), MOR after thermal shock from room temperature to 1 000 °C and HMOR after coking at 1 000 °C (c), theoretical crack initiation energy $\gamma_{NBT,th.}$ and theoretical crack propagation energy $\gamma_{WOF,th.}$ according to Eqn. (4) – (5) (d).

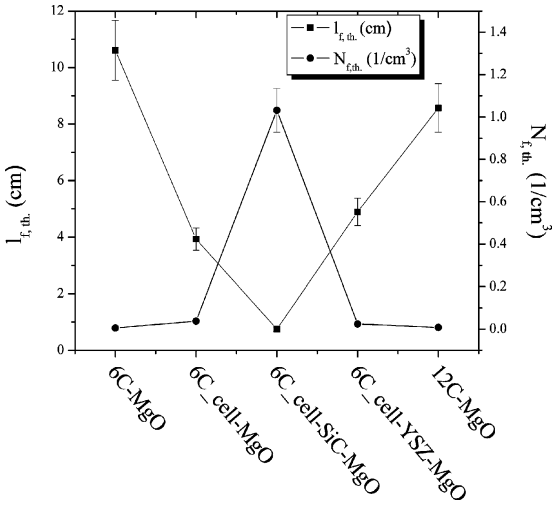

Fig. 5 : Calculated final crack length and final crack density values of hybrid carbon foams coated with SiC and YSZ and MgO infiltrated with MgO matrices as well as a pitch-bonded MgO-C reference refractory material (12C-MgO).

support, the different influencing factors for the optimization of thermomechanical high temperature characteristics according to the specific boundary conditions given by the specific model case of cellular hybrid carbon composites under investigation. Finally, in order to completely ascertain and confirm the applicability of the approximated thermal shock parameters, it is necessary that the most important parameters, e.g., γ_{WOF}, Young's moduli after thermal shock treatment, as well as the critical stress intensity factors are experimentally proven. Nevertheless, the underlying experimentally determined data and applied theories give practical and useful indications of first-approach evaluation of thermal shock characteristics as a function of underlying microstructural parameters.

(2) Thermomechanical modelling of size effects in MgO-C hybrid foams

Thermal shock behaviour

Fig. 6a shows an enlarged view of the computed stress distribution in the microstructure after the thermal shock

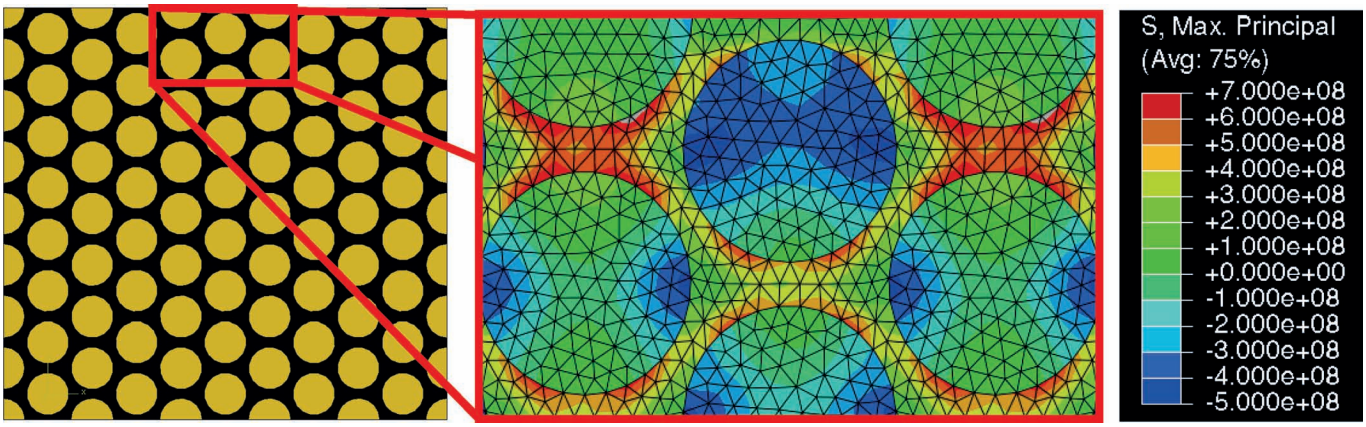

Fig. 6 : Reference RVE (100 % type) and image detail of the maximal principal stress distribution.

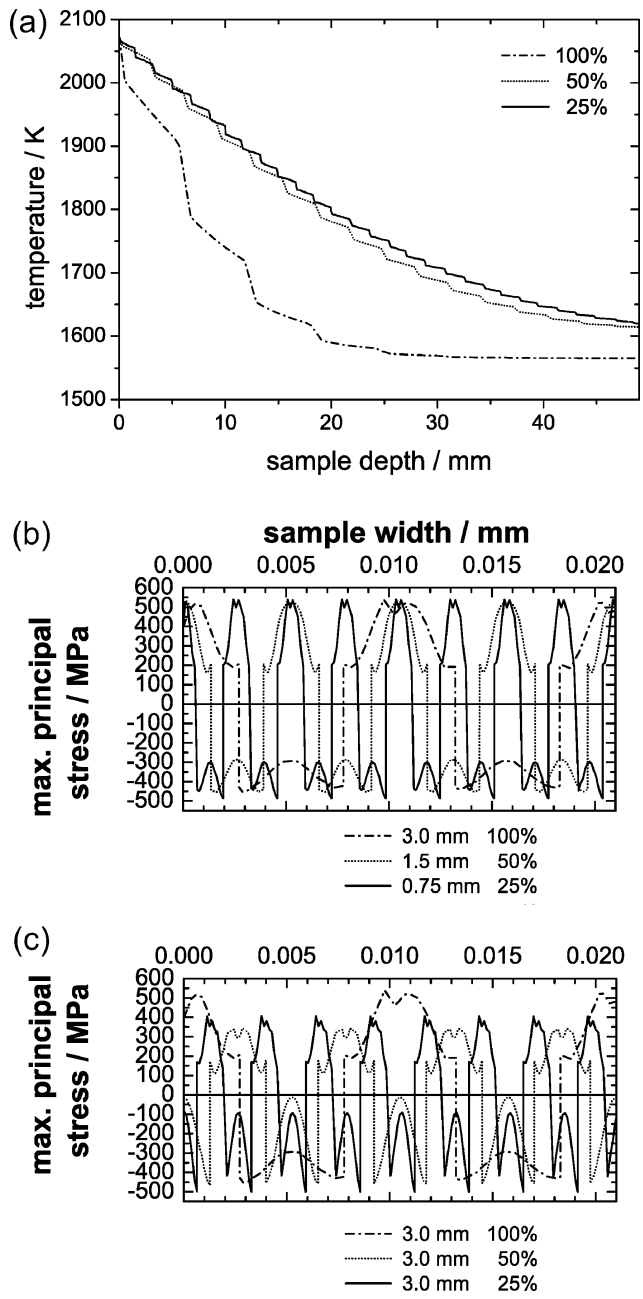

Fig. 7 : Temperature distribution (a) and maximal principal stresses in the first struts (b) and at a depth of 3.0 mm (c) as a function of the microstructural size.

loading. Compressive stresses are mainly concentrated in the periclase phase of the pores, whereas the struts are stressed by tensile stresses. Hence only the strut framework of the carbon foam phase is critical for damage. Size effects result from changes in the complete microstructural size. Fig. 7a shows the temperature distribution as a function of the sample depth for the three different microstructural sizes. The thermal shock loading causes large temperature gradients in the hybrid refractories. The reduction of the microstructure from 100 % to 50 % significantly improves the homogeneity of the temperature distribution in the foam and hence reduces temperature gradients. Further shrinking of the complete microstructure (e.g. 25 %) further improves the homogeneity of the temperature distribution but the improvement is less significant. In Fig. 7b the averaged maximal principal stresses after the thermal shock were computed for the first whole struts for each of the three microstructural sizes. Fig. 7c shows the corresponding stress distribution at a depth of 3.0 mm, which corresponds to the first strut of the 100 % type after the thermal shock. In spite of the higher temperature for both shrunken microstructures at an equal distance from the top side, the occurring stresses are significantly reduced in comparison to the reference RVE of 100 %. At the same microstructural locations, i.e. in the first pore layer measured from the top side for all investigated RVEs, the stress is the same, but due to the smaller size of the microstructure only a reduced fraction of the complete cellular hybrid refractory is affected by this large stress. In conclusion a reduction of the complete microstructure is favourable to improving the thermal shock resistivity. The temperature distribution is more homogeneous; the temperature gradients after the applied thermal shock are less pronounced.

In order to compare the results with the experimentally motivated thermal shock theory of Hasselman, the maximal principal stresses and the local temperatures at the struts are averaged over a rectangular reference region with an edge length that corresponds to the strut thickness. For the evaluation of the computed results in a Hasselman-like manner, the maximal principal stresses are plotted as functions of the temperature differences ΔT. The temperature differences are extracted from the results by determining the averaged temperature at different depth posi-

tions in the RVE. Fig. 8 shows the maximal principle stress in the struts as a function of the temperature difference ΔT for the 100 % and the 50 % types of the microstructure.

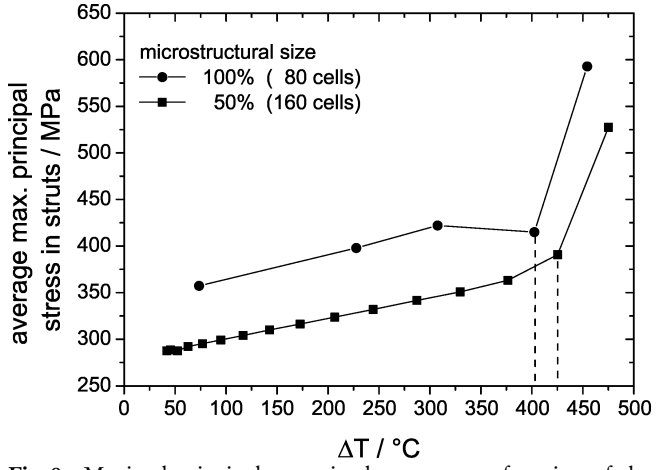

Fig. 8 : Maximal principal stress in the struts as a function of the temperature difference for different microstructural sizes.

There is a slight rise up to a critical temperature difference ΔT_C when the stress rises steeply. In comparison with Hasselman's classical thermal shock theory, the first region with slightly increasing stress causes no crack growth and hence no change in the residual strength of the refractory. The steep increase in stress at the critical temperature difference is associated with crack initiation, the instantaneous change in crack length, and discontinuous decrease in residual strength by Hasselman. The simplified model used correlates very well with Hasselman's theory, whereas the average maximal principal stress is considered a damage criterion and leads to the reversal of traditional Hasselman curve shape, since the maximal occurring stress is inversely related to the classically used residual strength.

A reduction in microstructural size by 50 % leads to a reduction of the average tensile stresses in the struts by 12 % to 25 %. The stress increase now shows a size effect. The critical temperature difference where stress rises steeply is approximately the same for both RVEs and amounts to about 410 K. In summary, a decreasing microstructural size reduces the critical stresses in the composite and is preferable for the microstructural design of cellular MgO-C hybrid refractories.

(3) Influence of quasistatic heating temperature and size effects on failure stresses in bending

Fig. 9 outlines the evolution of permanent thermal stresses in the hybrid foams due to the quasistatic heating by the difference in the CTEs for the 100 % and the 50 % types of the microstructure. According to the results of the computational thermal shock experiments after the quasistatic heating in the periclase phase of the pores, there are only compressive stresses that slightly increase with increasing final heating temperature. The carbon-based strut framework is solely loaded by thermally induced tensile stresses, which arise five times faster than the compressive stresses of the pores. Owing to the absence of temperature gradients based on the quasistatic heating, damage in this stage occurs only by permanent thermal stresses induced by the pairing of materials with highly different CTEs. There is no thermal shock damage or mechanical damage. Up to a final heating temperature of 850 °C the averaged maximal principal stresses are below the tensile strength of vitreous carbon and periclase, hence no damage occurs. At higher temperatures damage already occurs as a result of the quasistatic heating owing to permanent thermal stresses. Size effects due to a reduced microstructural size are negligible.

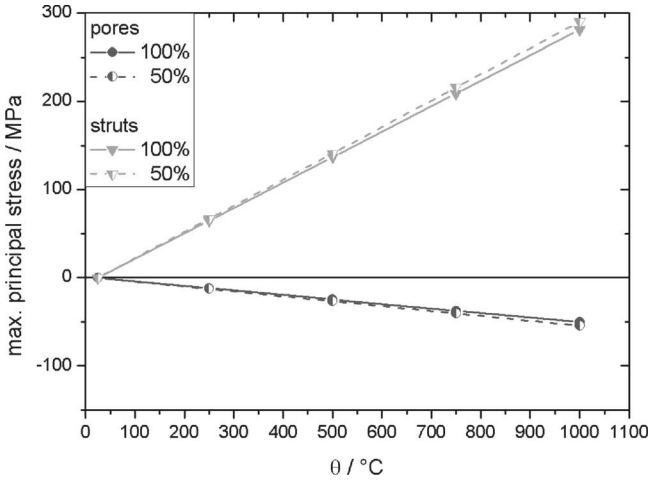

Fig. 9 : Averaged maximal principal stress in the pores and in the struts as a function of the final heating temperature for different microstructural sizes.

In the bending experiment the stresses in the pores and struts at the top and bottom side of the beam respectively are no longer equal (see Fig. 10) owing to the effect of bending, where the highest compressive stresses arise at the top and large tensile stresses at the bottom side of the beam. The horizontal centre line is the neutral fibre, where the stresses caused by the bending are zero. In comparison with the situation after the quasistatic heating, the stresses in the struts at the bottom side of the beam are increased by about 30 %. The reduction at the top side amounts to 8 %. The difference in stress $\Delta\sigma$ between the top and the bottom side ranges from 72 MPa to 108 MPa and hence is nearly independent of the final heating temperature. A final heating temperature above 680 °C will result in damage in the struts at the bottom side. Below this temperature the MgO-C hybrid refractory will be undamaged after bending.

Whereas after quasistatic heating the pores have to bear only non-critical compressive stresses, after bending there is also the stress split between the top and bottom of the beam and moreover, the stresses at the bottom side change to tensile stresses. The stress in the pores at the top remains compressive and nearly unchanged in comparison to the situation after the quasistatic heating. By increasing the final heating temperature, the gap $\Delta\sigma$ becomes larger. In ambient temperature $\Delta\sigma$ amounts to 100 MPa and increases up to 240 MPa. In the investigated temperature regime the stresses remain non-critical but at a temperature of about 1 100 °C there could be damage in the pores too. As for the quasistatic heating, size effects from a reduction in the microstructure are negligible.

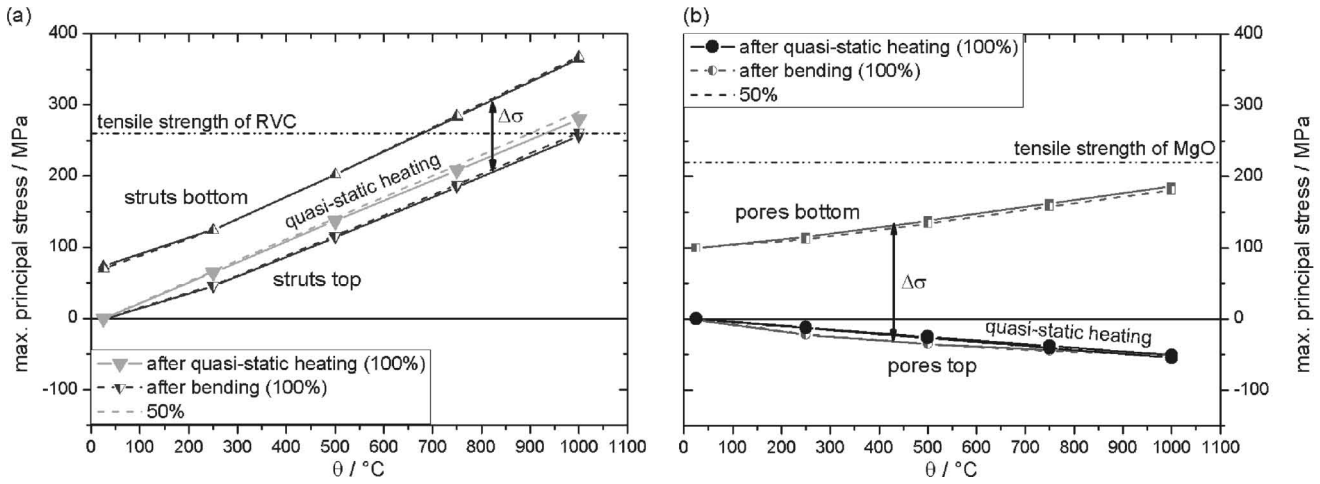

Fig. 10 : Averaged maximal principal stress in the struts (a) and in the pores (b) after quasistatic heating and after bending as a function of the final heating temperature for different microstructural sizes.

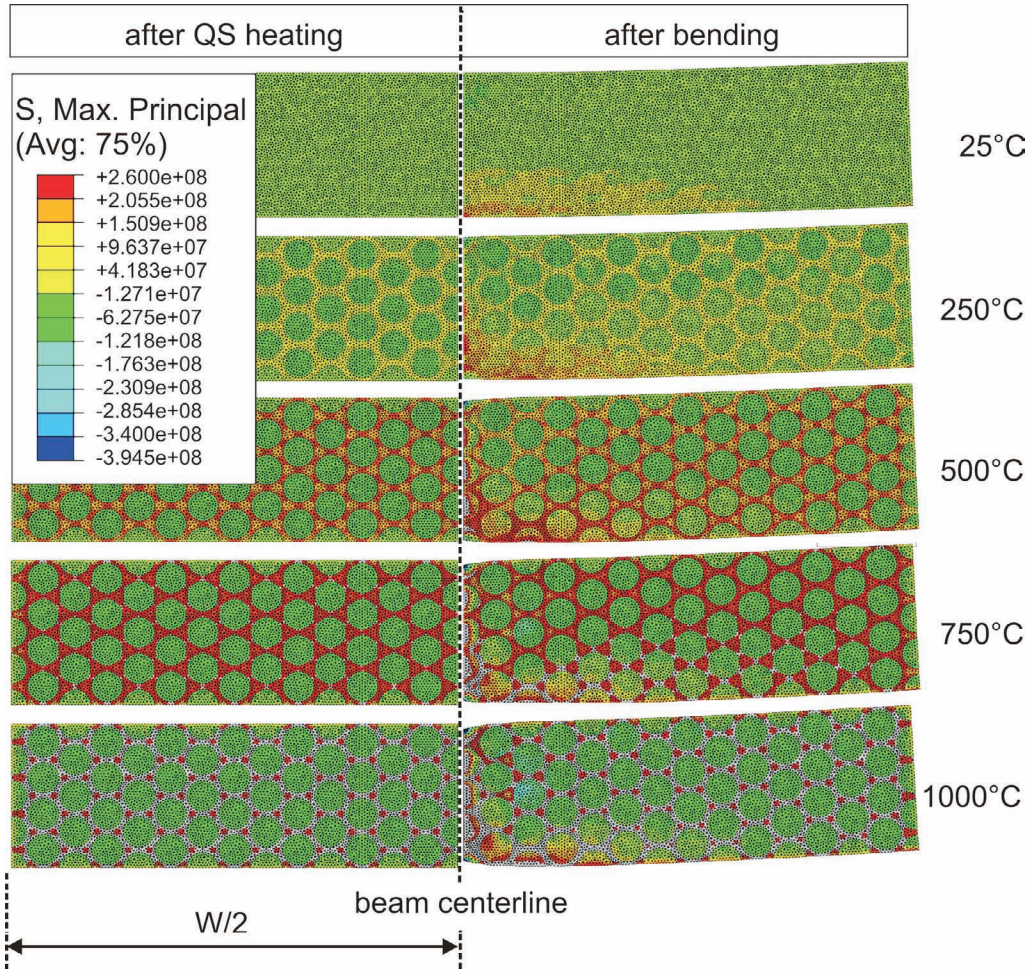

Fig. 11 : Spatial distribution of maximal principal stress in the 100 % type microstructure after quasistatic heating (left) and after bending (right) for different final heating temperatures. The grey colour belongs to elements where the stresses exceed the tensile stresses of the struts and pores, respectively.

Fig. 11 shows the spatial distribution of the computed maximal principal stresses for the microstructure of the 100 % type. The reference temperature is 25 °C there are no thermally induced stresses. Up to 500 °C the stress in the struts increases without exceeding the tensile strength. At a final temperature of 750 °C there are some damaged spots at the centre of the struts. At a temperature of 1 000 °C almost the complete carbon phase exceeds the tensile strength. Under bending there is the typical increase in tensile stress visible at the bottom for 25 °C. In this case, the stresses are from mechanical type and only result from the bending. For the higher temperatures,

the stresses are a superposition of the permanent thermal stresses and bending stresses. At 500 °C damage begins in the pores at the beam centre, where the displacement is applied. The localized early excess of tensile stress at the beam centre is caused by sheer stresses in this region, which increase with increasing heating temperature. Whereas before the bending at a temperature of 750 °C the struts are nearly completely undamaged, the bending step causes extensive damage at the bottom. Owing to the fact that the used model is based on linear elastic theory, stresses could be reduced with the application of the counter stresses. This is the case with bending. It can be demonstrated that the damaged regions at 1 000 °C after bending are smaller than before the bending.

V. Conclusions

In order to be able to tailor thermomechanical properties of reinforced and functionalized carbon foam materials for high-temperature refractory applications, yttria-stabilized zirconia (YSZ) and silicon carbide as model systems were deposited onto RVC structures by gel casting. Specific thermomechanical data have been experimentally determined and thermal shock parameters have been modelled based on these experimentally proven characteristics. The results are as follows:

1. Nano-sized YSZ and silicon carbide particles can be deposited onto the surface of cellular RVC substrates by co-immersion/compression.
2. The use of smart reinforcing materials doped in small quantities (i.e. 8YSZ, SiC) could offer a cost-effective approach for optimized hybrid carbon foam refractories, preventing slag penetration into the brick microstructure.
3. Thermomechanical data and approximated thermal shock parameters of hybrid carbon foam materials under investigation show that an overall elevated porosity and a resulting decrease of flexural strength, decreased modulus of elasticity as well as decreased modulus of rupture would result in significantly reduced crack initiation and crack propagation energy and would therefore cause an overall reduced thermal shock resistivity. The processing of well-designed pore sizes as well as pore distributions is indispensable to ensure the potentials of reinforced and functionalized cellular carbon hybrid materials as high-temperature refractories with advanced thermal shock resistivity and improved environmentally beneficial qualities.

FEM-based computational modelling has been performed in order to optimize microstructural cell parameters of MgO-C hybrid foams for advanced thermal shock applications and high-temperature applications without thermal shock. The concluding results of the numerical analysis are as follows.

By combining the experimentally motivated Hasselman equation with a simplified linear elastic thermomechanical approach, it is possible to qualitatively predict crack initiation and failure in cellular-based MgO-C hybrid refractories.

Based on the only elastic character of the model lacking a real damage criterion, stresses cannot be reduced by crack initiation and increasing crack density, hence the model overestimates the real situation for the thermal shock experiments.

Nevertheless, with this simplified model it is possible to qualitatively predict the behaviour of refractories with a complex microstructure.

The simulations show that tensile stresses arise only in the struts, whereas the pores are stressed by compressive stresses. The results of this very simplified modelling approach correlate very well with the experimentally motivated Hasselman theory.

It could be shown that under thermal shock loading a reduction in the microstructural size reduces the occurring stresses and hence the damage caused by temperature gradients. The simplified model has also been applied to quasistatic-heated bending beams. In this case thermal damage only occurs by permanent thermal stresses owing to the combination of materials that differ in their CTE. Through the superposition of these thermal stresses with bending stresses, size effects from changes in the microstructural size are negligible. It was possible to predict the temperature at which damage occurs with the FE analysis. In future work, the model should be extended with a real damage criterion accounting for stress release by crack initiation in order to not only qualitatively but also quantitatively correct computational results.

Acknowledgements

The authors gratefully acknowledge the support and funding of the German Research Foundation (DFG) grant no. FA 480/3 – 2 within the priority programme DFG-SPP 1418 "Refractories – Initiative to Reduce Emission – FIRE".

References

1 Krass, Y. R.: World production fo steel and magnesia refractories: State of the art and trends of development, Refractories and Industrial Ceramics, **42**, 417 – 425, (2001).

2 Ceylantekin, R., Aksel, C.: Improvements on the mechanical properties and thermal shock behaviours of MgO-spinel composite refractories by ZrO_2 incorporation, Ceramics International, **38**, 995 – 1002, (2012).

3 Yarushina, T. V., Akbashev, V. A., Plyukhin, V. A., Akbashev, A. M., Gyrlya, I. M., Parshikov, A. N.: Periclase-carbon composite refractories with new complex binder, Refractories and Industrial Ceramics, **48**, 170 – 175, (2007).

4 Suvorov, S. A., Mozhzherin, A. V., Sakulin, A. V., Ordin, V. G., Rusinova, E. V.: Functional carbonized refractories, ibid. **46**, 268 – 272, (2005).

5 Perepelitsyn, V. A., Kutalov, V. G.: Efficient refractory materials for metallurgy and casting production, ibid. **53**, 50 – 53, (2012).

6 Gallego, N. C., Klett, J. W.: Carbon foams for thermal management, Carbon, **41**, 1461 – 1466, (2003).

7 Chen, C., Kennel, E. B., Stiller, A. H., Stansberry, P. G., Zondlo, J. W.: Carbon foam derived from various precursors, ibid. **44**, 1535 – 1543, (2006).

8 Li, S., Tian, Y., Zhong, Y., Yan, X., Song, Y., Guo, Q., Shi, J., Liu, L.: Formation mechanism of carbon foams derived from mesophase pitch, ibid. 49, 618 – 624, (2011).

9 Inagaki, M., Morishita, T., Kuno, A., Kito, T., Hirano, M., Suwa, T., Kusakawa, K.: Carbon foams prepared from polyimide using urethane foam template, ibid. **42**, 497 – 502, (2004).

[10] Lei, S., Guo, Q., Shi, J., Liu, L.: Preparation of phenolic-based carbon foam with controllable pore structure and high compressive strength, ibid. **48**, 2644 – 2673, (2010).

[11] Chen, Y., Chen, B.-Z., Shi, X.-C., Xu, H., Hu, Y.-J., Yuan, Y., Shen, N.-B.: Preparation of pitch-based carbon foam using polyurethane foam template, ibid. **45**, 2126 – 2139, (2007).

[12] Li, X., Basso, M. C., Braghiroli, F. L., Fierro, V., Pizzi, A., Celzard, A.: Tailoring the structure of cellular vitreous carbon foams, ibid. **50**, 2026 – 2036, (2012).

[13] Sanchez-Coronado, J., Chung, D. D. L.: Thermomechanical behavior of a graphite foam, ibid. **41**, 1175 – 1180, (2003).

[14] Celzard, A., Tondi, G., Lacroix, D., Jeandel, G., Monod, B., Fierro, V., Pizzi, A.: Radiative properties of tannin-based, glasslike, carbon foams, ibid. **50**, 4102 – 4113, (2012).

[15] Gaies, D., Faber, K. T.: Thermal properties of pitch-derived graphite foam, ibid. **40**, 1131 – 1150, (2002).

[16] Latella, B. A., Liu, T.: The initiation and propagation of thermal shock cracks in graphite, ibid. **44**, 3043 – 3048, (2006).

[17] Qiu, H., Han, L., Liu, L.: Properties and microstructure of graphitised ZrC/C or SiC/C composites, ibid. **43**, 1021 – 1025, (2005).

[18] Bag, M., Adak, S., Sarkar, R.: Study on low carbon containing MgO-C refractory: Use of nano carbon, Ceramics International, **38**, 2339 – 2346, (2012).

[19] Silveira, W. D., Falk, G.: Production of refractory materials with cellular matrix by colloidal processing, Refractories Worldforum, **4**, 143 – 150, (2012).

[20] Silveira, W. d., Falk, G.: Reinforced cellular carbon matrix-MgO composites for high temperature appliactions: Microstructure aspects and colloidal processing, Adv. Eng. Mat., **13**, 982 – 989, (2011).

[21] Damhof, F., Brekelmans, W. A. M., Geers, M. G. D.: Non-local modelling of cyclic thermal shock damage including parameter estimation, Eng. Fract. Mech., **78**, 1846 – 1861, (2011).

[22] Damhof, F., Brekelmans, W. A. M., Geers, M. G. D.: Non-local modeling of thermal shock damage in refractory materials, Eng. Fract. Mech., **75**, 4706 – 4720, (2008).

[23] Harmuth, H., Rieder, K., Krobath, M., Tschegg, E.: Investigation of the nonlinear fracture behaviour of ordinary ceramic refractory materials, Mat. Sci. Eng. A, **214**, 53 – 61, (1996).

[24] Lu, T. J., Fleck, N. A.: The thermal shock resistance of solids, Acta Mater., **46**, 4755 – 4768, (1998).

[25] Hartmuth, H., Tschegg, E. K.: A fracture mechanics approach for the development of refractory materials with reduced brittleness, Fatigue Fract. Engng. Mater. Struct., **20**, 1585 – 1603, (1997).

[26] Orenstein, R. M., Green, D. J.: Thermal shock behavior of open-cell ceramic foams, J. Am. Ceram. Soc., **75**, 1899 – 1905, (1992).

[27] Swain, M. V.: R-Curve behavior and thermal shock resistance of ceramics, ibid. **73**, 621 – 628, (1990).

[28] Hasselmann, D. P. H.: Unified Theory of thermal shock fracture initiation and crack propagation in brittle ceramics, J. Am Ceram. Soc., **52**, 600 – 604, (1969).

[29] Salvini, V. R., Pandolfelli, V. C., Bradt, R. C.: Extension of Hasselman's thermal shock theory for crack/microstructure interactions in refractories, Ceramics International, **38**, 5369 – 5375, (2012).

[30] Grasset-Bourdel, R., Alzina, A., Huger, M., Gruber, D., Harmuth, H., Chotard, T.: Influence of thermal damage occurrence at microstructural scale on the thermomechanical behaviour of magnesia-spinel refractories, J. Europ. Ceram. Soc., **32**, 989 – 999, (2012).

[31] Schmitt, N., Burr, A., Berthaud, Y., Poirier, J.: Micromechanics applied to the thermal shock behavior of refractory ceramics, Mechanics of Materials, **34**, 725 – 747, (2002).

[32] Jiang, J.-W., Wang, J.-S., Li, B.: Thermal expansion in single-walled carbon nanotubes and graphene: Nonequilibrium Green's function approach, Phys. Rev. B, **80**, 205429, (2009).

[33] Dubrovinsky, L. S., Saxena, S. K.: Thermal expansion of Periclase (MgO) and Tungsten (W) to melting temperatures, Phys. Chem. Minerals, **24**, 547 – 550, (1997).

[34] Mei, H., Cheng, L., Zhang, L., Xu, Y.: Modeling the effects of thermal and mechanical load cycling on a C/SiC composite in oxygen/argon mixtures, Carbon, **45**, 2195 – 2204, (2007).

[35] Diebels, S., Steeb, H.: The size effect in foams and its theoretical and numerical investigation, The Royal Society Proceedings: Mathematical, Physical and Engineering Sciences, **458**, 2869 – 2883, (2002).

[36] Nieh, T. G., Higashi, K., Wadsworth, J.: Effect of cell morphology on the compressive properties of open-cell aluminum foams, Materials Science and Engineering A, **283**, 105 – 110, (2000).

[37] Onck, P. R., Andrews, E. W., Gibson, L. J.: Size effects in ductile cellular solids. Part I: Modeling, Inter. J. Mech. Sci., **43**, 681 – 699, (2001).

[38] Tekoglu, C., Gibson, L. J., Pardoen, T., Onck, P. R.: Size effects in foams: Experiments and modeling, Progress in Materials Science, **56**, 109 – 138, (2011).

[39] Christensen, R. M.: Mechanics of low density materials, J. Mech. Phys. Solids, **34**, 563 – 578, (1986).

[40] Gent, A. N., Thomas, A. G.: The formation of foamed elastic materials, J. Appl. Polymer Sci., **1**, 107 – 113, (1959).

[41] Gibson, L. J., Ashby, M. F., and, G. S. S., Robertson, C. I.: The mechanics of two-dimensional cellular materials, Proc. R. Soc. London, Ser. A, **A 382**, 25 – 42, (1986).

[42] Meguid, S. A., Cheon, S. S., El-Abbasi, N.: FE modelling of deformation localization in metallic foams, Finite Elem. Anal. Des., **38**, 631 – 643, (2002).

[43] Warren, W. E., Kraynik, A. M.: The linear elastic properties of open-cell foams, J. Appl. Mech., **55**, 341 – 346, (1988).

[44] Deshpande, V. S., Fleck, N. A.: Isotropic constitutive models for metallic foams, J. Mech. Phys. Solids, **48**, 1253 – 1283, (2000).

[45] Diebels, S.: A macroscopic description of the quasi-static behavior of granular materials based on the theory of porous media, Granul. Matter, **2**, 142 – 152, (2000).

[46] Diebels, S., Steeb, H., Ehlers, W.: Microscopic and macroscopic modelling of foams, Proc. Appl. Math. Mech., **2**, 156 – 157, (2003).

[47] Ehlers, W.: A single-surface yield function for geomaterials, Arch. Appl. Mech., **65**, 246 – 259, (1995).

[48] Klett, J., Lowden, R., McMillan, A.: Oxidation protection of graphite foams, Oak Ridge National Laboratory, 2001.

[49] Hasselmann, D. P. H.: Strength behavior of polycrystalline alumina subjected to thermal shock, J. Am. Ceram. Soc., **53**, 490 – 495, (1970).

[50] Hasselman, D. P. H., Youngblood, G. E.: Enhanced thermal stress resistance of structural ceramics with thermal conductivity gradient, J. Am. Ceram. Soc., **61**, 49 – 52, (1978).

[51] Hasselman, D. P. H., Badaliance, R., Chen, E. P.: Thermal fatigue and its failure prediction for brittle ceramics. In: Thermal Fatigue of Materials and Components. 1976.

[52] Lu, T. J., Fleck, N. A.: The thermal shock resistance of solids, Acta Mater., **46**, 4755 – 4768, (1998).

[53] Bahr, H.-A., Balke, H.: Fracture analysis of a single edge cracked strip under thermal shock, Theoretical and Applied Fracture Mechanics, **8**, 33 – 39, (1987).

[54] Balke, H., Hofinger, I., Häusler, C., Bahr, H.-A., Weiß, H.-J., Kirchhoff, G.: Fracture mechanical damage modelling of thermal barrier coatings, Arch. Appl. Mech., **70**, 193 – 200, (2000).

[55] Cotterel, W. O., Ong, S. W., Qin, C.: Thermal Shock and Size Effects in Castable Refractories, J. Am. Ceram. Soc., **78**, 2056 – 2064, (1995).

[56] Soboyejo, W. O., Mercer, C.: Investigation of thermal shock in a high-temperature refractory ceramic: A fracture mechanics approach, J. Am. Ceram. Soc., **84**, 1309 – 1314, (2001).

[57] Damhof, F., Brekelmans, W. A. M., Geers, M. G. D.: Predictive FEM simulation of thermal shock damage in the refractory lining of steelmaking installations, J. Mat. Proc. Tech., **211**, 2091 – 2105, (2011).

[58] Bradley, F., Chaklader, A., Mitchell, A.: Thermal stress fracture of refractory lining components: Part I. Thermoelastic analysis, Metall. and Mater. Trans. B, **18**, 355 – 363, (1987).

[59] Knauder, J., Rathner, R.: Thermomechanical analysis of basic refractories in a bottom blowing converter, Veitsch-Radex Rundschau, **4**, 354 – 364, (1990).

[60] Knauder, J., Rathner, R.: Improved design of a bof lining based on thermomechanical analysis,, Veitsch-Radex Rundschau, **1**, 203 – 212, (1990).

[61] Rathner, R., Knauder, J. P., Schweiger, H. F.: Lining design and behavior of BOF's, ibid. **4**, 327 – 342.

[62] Andreev, K., Harmuth, H.: FEM simulation of the thermomechanical behaviour and failure of refractories—a case study, J. Mater. Process. Technol., **143 – 144**, 72 – 77, (2003).

[63] Gruber, D., Andreev, K., Harmuth, H.: FEM simulation of the thermomechanical behaviour of the refractory lining of a blast furnace, J. Mater. Process. Technol., **155 – 156**, 1539 – 1543, (2004).

[64] Prompt, N., Ouedraogo, E.: High temperature mechanical characterisation of an alumina refractory concrete for Blast Furnace main trough. Part I. General context, J. Eur. Ceram. Soc., **28**, 2859 – 2865, (2008).

[65] Stabler, J., Baker, G.: Fractional step methods for thermo-mechanical damage analyses at transient elevated temperatures, Int. J. Num. Meth. Eng., **48**, 761 – 785, (2000).

[66] Luccioni, B. M., Figueroa, M. I., Danesi, R. F.: Thermo-mechanic model for concrete exposed to elevated temperatures, Eng. Struct., **25**, 729 – 742, (2003).

[67] Nechnech, W., Meftah, F., Reynouard, J. M.: An elasto-plastic damage model for plain concrete subjected to high temperatures, Eng. Strct., **24**, 597 – 611, (2002).

[68] Pearce, C. J., Nielsen, C. V., Bicanic, N.: Gradient enhanced thermo-mechanical damage model for concrete at high temperatures including transient thermal creep, Int. J. Numer. Anal. Meth. Geomech., **28**, 715 – 735, (2004).

[69] Stabler, J., Baker, G.: On the form of free energy and specific heat in coupled thermo-elasticity with isotropic damage, Int. J. of Solids and Structures, **37**, 4691 – 4713, (2000).

[70] Stabler, J., Baker, G.: Fractional step methods for thermo-mechanical damage analyses at transient elevated temperatures, Int. J. Numer. Math. Eng., **48**, 761 – 785, (2000).

[71] Pabst, W., Gregorova, E., Ticha, G.: Elasticity of porous ceramics—A critical study of modulus-porosity relations, J. Eur. Ceram. Soc., **26**, 1085 – 1097, (2006).